V European Conference on Computational Fluid Dynamics
ECCOMAS CFD 2010
J. C. F. Pereira and A. Sequeira (Eds)
Lisbon, Portugal, 14–17 June 2010

APPLICABILITY OF RANS MODELS FOR ACCURATE COMPUTATION OF FLOW OVER AIRFOILS WITH SERRATED TRAILING EDGES (ECCOMAS CFD 2010)

Gerson C. Fernandes[*], Markus Weinmann[*], and Richard D. Sandberg[*]

[*]School of Engineering Sciences, University of Southampton
Southampton, SO17 1BJ, United Kingdom
e-mail: sandberg@soton.ac.uk

Key words: Fluid Dynamics, Airfoil Noise, RANS, Trailing-edge Serrations

Abstract. *This paper investigates the applicability of RANS-based turbulence models for computation of flow over airfoils with serrated trailing edges. A precise representation of the hydrodynamic field in the vicinity of trailing-edge modifications is the essential if reliable noise predictions were to be employed in the design process of quieter airfoils. Simulations of NACA-0012 airfoils at* $Re_C=1.06\times10^6$ *with unserrated and serrated trailing-edge extensions were conducted using three RANS models employing an eddy-viscosity approximation, namely S-A, realizable* K-ε *and* K-ω *SST, and two nonlinear explicit algebraic Reynolds stress models. Our results indicate that the RANS closures are able to predict strong variations in the mean flow and statistical quantities due to the presence of trailing-edge serrations. Nevertheless, the predicted values are strongly dependent on which turbulence model is employed, suggesting that any noise prediction model would exhibit a considerable sensitivity to the choice of turbulence model. No drag penalty was observed for serrated trailing edges.*

1 INTRODUCTION

Noise has become an important design driver in many engineering applications. Airfoil self-noise, caused by the interaction of the boundary layers and wake produced with the airfoil itself, constitutes an important fraction of the total noise produced by aerodynamic surfaces. In Brooks *et al.*[1], the majority of sources of airfoil self noise were attributed to the trailing-edge noise mechanism. This noise generation mechanism is the result of fluctuations passing over a geometrical discontinuity, here a sharp edge, causing scattering which results in an increase in the radiated sound power scaling to M^5,[2] compared with M^8 in freestream turbulence[3].

Trailing edge noise is therefore considered the predominant noise source, particularly at low Mach number. Trailing edges with their associated noise are widely present in many devices, from airplanes to wind turbines and rotors to fans. The ever tightening regulations on both noise and emissions have set on the quest for silent aircraft. The Advisory Council for Aeronautics in Europe (ACARE) in its “Vision for 2020” statement with its associated Strategic Research Agenda (SRA) have set noise targets of

10 EPNdB noise reduction for new aircraft entering service in 2020 as compared to a year 2000 ‘datum’ level. A 10dB reduction on the logarithmic EPNL scale implies an order of magnitude reduction in radiated sound power, in turn implying the necessity for the implementation of new noise reduction technologies[4].

Alongside aircraft noise, the noise radiated from wind turbines is a major hindrance for the widespread use of wind energy, a clean and practically inexhaustible source of energy[5]. Van den Berg *et al.*[6] conducted a survey in the Netherlands concluding that the most significant factor pertaining to the annoyance of wind farms is noise.

Wind tunnel experiments by Bohn[7], Fink and Bailey[8], Herr *et al*.[9], amongst others, proved that flow permeable edge extensions, such as porous edges or brushes are effective in reducing trailing-edge noise. Howe[10] studied flat plates with ‘saw tooth’-like trailing edges, predicting that the intensity of trailing-edge noise radiation would be attenuated by this geometry, with the magnitude of the reduction being a function of the length and spanwise spacing of the teeth, and the frequency of the radiation. It was determined that longer, narrower teeth should yield a greater intensity reduction.

Experimental work on a 2.3 MW prototype wind turbine, with a 94m diameter rotor and a tower height of 100m, was conducted by Oerlemans *et al.*[11]. In this study, a standard blade was compared to an optimised and a serrated blade. The noise emitted was reduced by 0.5 dB and 3.2dB for the optimised blade and the serrated blade, respectively. Crucially, the addition of the trailing-edge serrations was not found to alter the aerodynamic performance of the blade.

Whilst this reduction in noise at no aerodynamic expense is very encouraging, the explanation for this noise reducing mechanism and flow physics behind this gain are not yet explicitly quantified. In an attempt to investigate the flow in the vicinity of the trailing-edge serrations in detail, direct numerical simulations (DNS) employing a novel immersed boundary method were performed by Jones and Sandberg[12]. This study confirmed that the addition of serrations reduces the amplitude of trailing-edge noise over a finite frequency band.

Although DNS can shed some light into the detailed noise attenuation mechanisms of trailing-edge modifications, this method is still prohibitively expensive for practical Reynolds numbers, in particular in a low-noise airfoil design methodology. To overcome the problem of excessive computational cost, there have recently been attempts at developing RANS-based noise prediction methods. In these methods, either the surface pressure spectrum is empirically modelled based on turbulent scales obtained from RANS simulations[13], or stochastic methods for generating 4D spatio-temporal synthetic turbulence are employed[14]. In addition, these models require mean flow values, such as streamwise velocity component and boundary layer thickness. Undoubtedly, these lower-cost models will rely on the quality of the turbulence scales predictions and have so far not been employed for trailing edges with geometric modifications.

Therefore, this paper aims at evaluating whether RANS-based methods can be relied upon for calculation of the flow over airfoils with trailing-edge serrations that could serve as input for noise predictions. For RANS-based noise prediction tools of serrated airfoil geometries to be reliable, the computed flow field and turbulence quantities must exhibit variations due to the geometrical modification. Due to the lack of detailed data of the flow in the vicinity of trailing-edge serrations obtained from experiments or high-accuracy unsteady methods, solutions from the various RANS-based models used can only be compared to each other or to a reference case without serrations. All RANS calculations were conducted using the commercial flow solver STAR-CCM+ and the public domain solver OpenFOAM.

2 SCHEMES AND SOLVER SETTINGS

The Reynolds number, based on freestream velocity and airfoil chord, was chosen to be Re_C=1.06×10^6 when using a free stream velocity of 15.14 m/s. Because the Mach number at this low velocity was approximately 0.05, it was decided to conduct incompressible simulations. Following this decision, the governing equations of the velocity components and pressure were set to be solved in an uncoupled manner using the segregated flow model. The momentum and continuity equations are linked with a predictor-corrector approach. The formulation in the solver uses a collocated variable arrangement, as opposed to a staggered approach, and a Rhie and Chow-type pressure-velocity coupling combined with a SIMPLE-type algorithm was utilized. For all calculations conducted, the second-order accurate upwind convection scheme option was chosen for the spatial finite volume discretization[15].

The choice of the segregated approach is appropriate for the current flow conditions as it is most appropriate for incompressible flows without large body forces and energy sources. Compared to the coupled approach, it has the advantage of being less computationally demanding.

The time integration was set to ‘steady’ because steady RANS calculations were performed. The motion model for the airfoil was set to be stationary, as no motion is to occur from the airfoil or any other boundary.

2.1 Possible inadequacy of the RANS approach

First derived by Reynolds in 1894, the RANS equations are derived from the full Navier-Stokes equations by conducting a Reynolds decomposition of the velocity field $u_k(x_k,t)$ into a fluctuating ($u_k{}'(x_k,t)$) and a mean ($\overline{u_k(x_k,t)}$) value as shown

$$u_k{}'(x_k,t) \equiv u_k(x_k,t) - \overline{u_k(x_k,t)}, \tag{1}$$

and then performing a time-average. The RANS equations, here for simplicity the streamwise momentum equation only, can then be written as

$$\begin{aligned}\frac{\partial\bar{u}}{\partial t} + \frac{\partial(\bar{u}\bar{u}+\overline{u'u'})}{\partial x} + \frac{\partial(\bar{u}\bar{v}+\overline{u'v'})}{\partial y} + \frac{\partial(\bar{u}\bar{w}+\overline{u'w'})}{\partial z} \\ = -\frac{1}{\rho}\frac{\partial\bar{p}}{\partial x} + \upsilon\left(\frac{\partial^2\bar{u}}{\partial x^2} + \frac{\partial^2\bar{u}}{\partial y^2} + \frac{\partial^2\bar{u}}{\partial z^2}\right),\end{aligned} \tag{2}$$

where the quantities $\overline{u_k{}'u_l{}'}$ are the unknown Reynolds stress tensor components. The challenge to solve the RANS equations is to model the Reynolds-stress components.

Most commercial CFD packages allow using either a full Reynolds-stress transport model or employing a so-called eddy-viscosity model. The Reynolds Stress Transport Model, also known as ‘second-moment closure models’, attempts to solve transport equations for each component of the Reynolds stress tensor. This is presumably the most accurate method, but it comes at the price of high computational expense and numerical stability issues. Alternatively, the eddy-viscosity model using the turbulent-viscosity hypothesis first proposed by Boussinesq in 1877 relates the deviatoric Reynolds stress tensor to the mean rate of strain in a linear fashion

$$-\rho\overline{u_k{}'u_l{}'} + \frac{2}{3}\rho k\delta_{kl} = 2\rho\nu_T\bar{S}_{kl}, \tag{3}$$

where ν_T is the turbulent viscosity or eddy viscosity. Equation 3 is used in the Spalart-Allmaras (S-A), K-ε and K-ω SST models. The Boussinesq hypothesis has been shown to be a reasonable approximation for many two dimensional mean flows. However, for the current case of trailing-edge serrations, the eddy-viscosity approximation may be inadequate because we expect genuine three-dimensional mean flow and it fails to predict turbulence-induced secondary flows. Therefore, the performance of two explicit algebraic stress model (EASM) formulations will be compared to the turbulence closures based on the eddy-viscosity assumption. The explicit algebraic stress model (EASM) is formally derived from a RSM using an equilibrium hypothesis and representation theory and consequently inherits some of the improved predictive capabilities of the 'parent' RSM. The formulation used here is based on the pressure-strain model of Speziale *et al.*[16] which is used in conjunction with the assumption of two-dimensional mean flow. Note that this assumption does not imply that the resulting model is not applicable in three-dimensional mean flow. In fact, previous studies have demonstrated that such formulations may produce very similar results in complex three-dimensional flows when compared to the much more complex three-dimensional EASM formulation[17]. The resulting non-linear stress strain relationship of the EASM is used within a K-ω framework[17].

In an attempt to improve the prediction of the stress tensor and anisotropy close to solid boundaries, the EASM is extended with improved wall modelling capabilities using an elliptic blending approach. The resulting model (**φ-α** EASM) employs additional near-wall anisotropy modification and a near-wall consistency constraint in order to correctly reproduce the highly anisotropic state and the limiting two component state of turbulence as the wall is approached. For more information the reader is referred to reference[18].

3. GRID & SIMULATION PARAMETERS

3.1 Geometry

The geometry studied consists of a NACA-0012 airfoil with a splitter plate of constant thickness ($1 \times 10^{-3}\ m$), span of $0.25m$ and length $0.1m$ attached to it. The properties of the original airfoil are maintained, and thus the trailing edge extension results in a total chord length of $1.096m$. The serrated plate was made by cutting triangles into the splitter plate. The length of the serration from root to tip is 0.0999m, and the full width of each serration is 0.1667m. The angle from the symmetry line of the serration (i.e. half-angle of the serration) to the side is 39.8°. The plan form area of the serrated airfoil is $0.2616\ \mathrm{m}^2$. A reference case with a shorter (0.0465 m), unserrated trailing-edge extension resulting in the same plan form area was also computed.

The choice of NACA-0012 airfoil allows for a simple yet widely documented geometry to be created. The thickness of the serrated plate was chosen to be sharp, rather than blunt, by adhering to the requirement of the ratio of the trailing-edge thickness to the local displacement thickness being less than 0.3.

3.2 Grid generation strategy

In order to improve the accuracy of the numerical predictions, the domain was discretized in a fully structured manner. The solutions obtained from RANS equations are highly dependent upon the quality of the grid and the goal here was to generate a mesh of sufficient quality that the computations would not improve with further refinement, i.e. the solution would be grid-independent. This was a crucial requirement for being able to compare the performance of individual RANS models to each other. At the same time, constraints in available computational resources had to be taken into account.

After initial attempts to produce unstructured meshes, which were much simpler to generate, it quickly became clear that they would not suit the requirements of adequate quality and reasonable computational cost, i.e. containing the lowest possible number of cells for given accuracy. The performance of unstructured meshes in commercially available software packages are improving constantly, partly due to the industry's demand of easier, more user friendly and quicker turnaround times of computational studies, and they might well become suited to the current problem in the near future. But currently a fully structured grid offers superior control of cell location, quality and distribution.

Therefore, a fully structured grid was developed for the current complex geometry using GRIDGEN. The first step was to correctly and adequately mesh a two dimensional NACA-0012 geometry. When designing a classical C-type grid, the aspect ratio of several cells in the far field increased to very high levels, thus not allowing the residuals of the flow simulations to converge adequately. Therefore, a slight modification to a classical C-type grid was chosen, shown in figure 1 (left), as it avoided that problem. Figure 1 (left) also shows the number of connectors employed to have full control of the distribution of points around the airfoil, and a detail of the trailing-edge region (figure 1, right) demonstrates the fine resolution in both the tangential and lateral directions. The dimensions of the full integration domain in all spatial directions are summarised in table 1. Upon assuring the quality of the two dimensional grid by comparison of the flow simulation results with reference data (see section 4), the 3D NACA-0012 grid was made by projecting the 2D grid in the spanwise (Z) direction using 30 points for the initial unserrated design. A splitter plate with

Direction	**Chord Lengths**	**Number of points**
X	$-4.6 \leq X \leq 7.3$	1236 (tangential)
Y	$-6.4 \leq Y \leq 6.4$	100 (lateral)
Z	$0 \leq Z \leq 0.3$	57-60 (spanwise)

Table 1 Spatial dimensions of domain for 2D and 3D unserrated simulation.

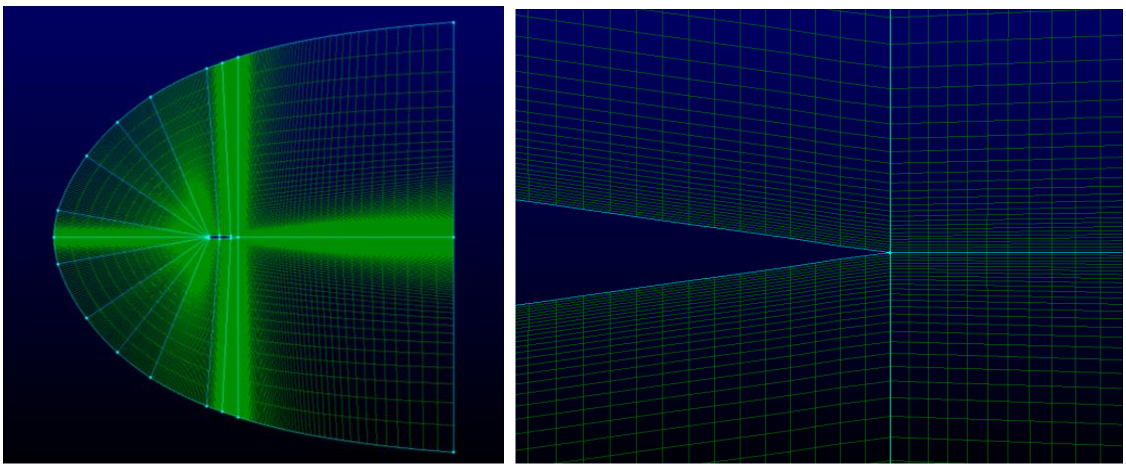

Figure 1: Topology of the mesh for a spanwise plane, showing the connectors used for mesh generation (top); detail of the fine grid resolution at the trailing edge (bottom).

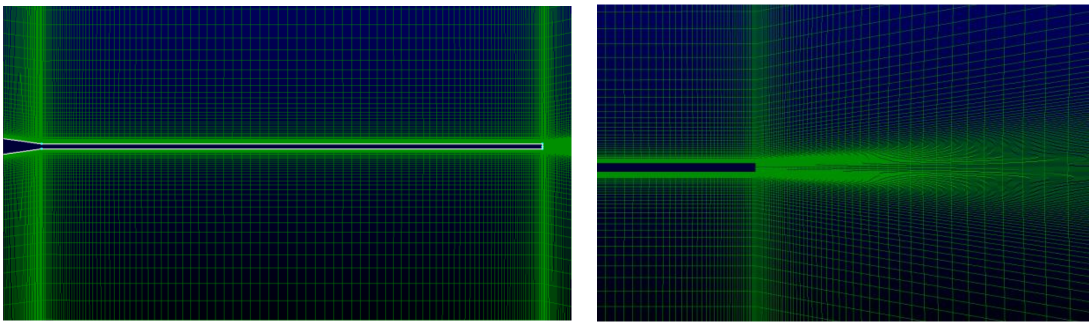

Figure 2: Topology of the mesh for a spanwise plane, showing the trailing-edge extension (left); detail of the fine grid resolution at the trailing edge of the flat-plate extension (right).

$1 \times 10^{-3}\, m$ thickness was then added to the trailing edge of the two dimensional NACA 0012, and meshed in a similar manner with 30 points across the thickness of the plate, and later projected into the third direction. While designing the mesh, the distance of the first grid point to the closest wall was estimated using XFOIL[19] predictions of the skin friction coefficient. The skin friction coefficient C_f is defined as $C_f = 2\tau_w/\rho U_\infty^2$, thus the friction velocity u_τ can be computed as $u_\tau = \sqrt{\tau_w/\rho}$ and the distance from the wall scaled in wall coordinates could be evaluated as $Y^+ = u_\tau y/\nu$. By relying on inexpensive XFOIL predicitions of C_f, an expensive procedure of iteratively improving the mesh after each RANS simulation could be avoided, and a-posteriori checks of the grid resolution at the wall in wall coordinates confirmed the initial estimates.

3.3 Simulation settings

The free stream values of turbulence quantities play an important role in determining the final flow solution, in particular for the S-A model. Setting unrealistically high values of, e.g., eddy viscosity at the freestream boundary will result in a poor prediction of lift and drag of the airfoil and making validation of the computational set-up and turbulence model choice impossible. The inlet and outlet boundary boundary conditions for the Spalart-Allmaras, K-ε and K-ω SST models were chosen as suggested by Spalart and Rumsey[20]. Values for the modified turbulent diffusivity $\tilde{\nu}$ were chosen to satisfy the ratio of $\tilde{\nu}/\nu = 3$, allowing the turbulent boundary layers on the airfoil to develop at reasonably high Reynolds number, while ensuring that ambient values do not influence the interior of the boundary layer. The eddy kinematic viscosity was set to $\nu_T = \mu_T/\rho = \tilde{\nu} f_{v1} = 3.274 \times 10^{-6}\, m^2/s$, where $f_{v1}$is a variable in the formulation of the S-A turbulence, corresponding to a turbulent viscosity ratio $\nu_T/\nu = 0.209$. These values correspond with those suggested by Spalart and Allmaras[21].

For the K-ε and K-ω SST models, the following freestream boundary conditions were specified: $k/u^2 = 1 \times 10^6$, $\epsilon c/u^3 = 4.5 \times 10^{-7}$, $\omega = 5u/c$, where $k = 2.292 \times 10^{-4} m^2/s^2, \epsilon = 1.4248 \times 10^{-7} m^3/s^2, \omega = 69.07\, 1/s, u = 15.14\, m/s,$ and $c = 1.096m$.

The approach taken here was to have a fully turbulent flow over the entire airfoil. This is not what would naturally occur at this Reynolds number, where laminar-turbulent transition would be expected. However RANS-based models are not well suited for accurate transition predictions and thus, as recommended by Spalart and Rumsey[20], a ‘fully turbulent’ approach was specified, giving better convergence.

4 VALIDATION

4.1 XFOIL

As a first step, the numerical set-up was validated by performing 2D RANS simulations of a NACA-0012 with and without trailing-edge extension and comparing the results to reference data obtained from XFOIL. This was deemed to be adequate because XFOIL predictions at the current Reynolds and Mach number and at zero incidence are quite accurate. XFOIL employs the e^N transition prediction method. In order to be consistent with the RANS predictions performed here, where turbulent flow was computed over the entire airfoil chord, in XFOIL the flow was tripped at the leading edge. For this Reynolds number, transition would otherwise occur at approximately 60% chord. The difference between tripped and untripped XFOIL predictions is significant, with the drag coefficient being C_D=0.00542 and C_D=0.01118 for the untripped and tripped cases, respectively.

To finally ensure the validity of XFOIL predictions, the C_L and C_D values were compared to experimental data for the same airfoil in Abbott and von Doenhoff[22] and are presented in figure 1. XFOIL is seen to compare well with the experimental data. Given that for the more complex untripped case the validation was successful, it was deemed that the simplified tripped case was a suitable reference.

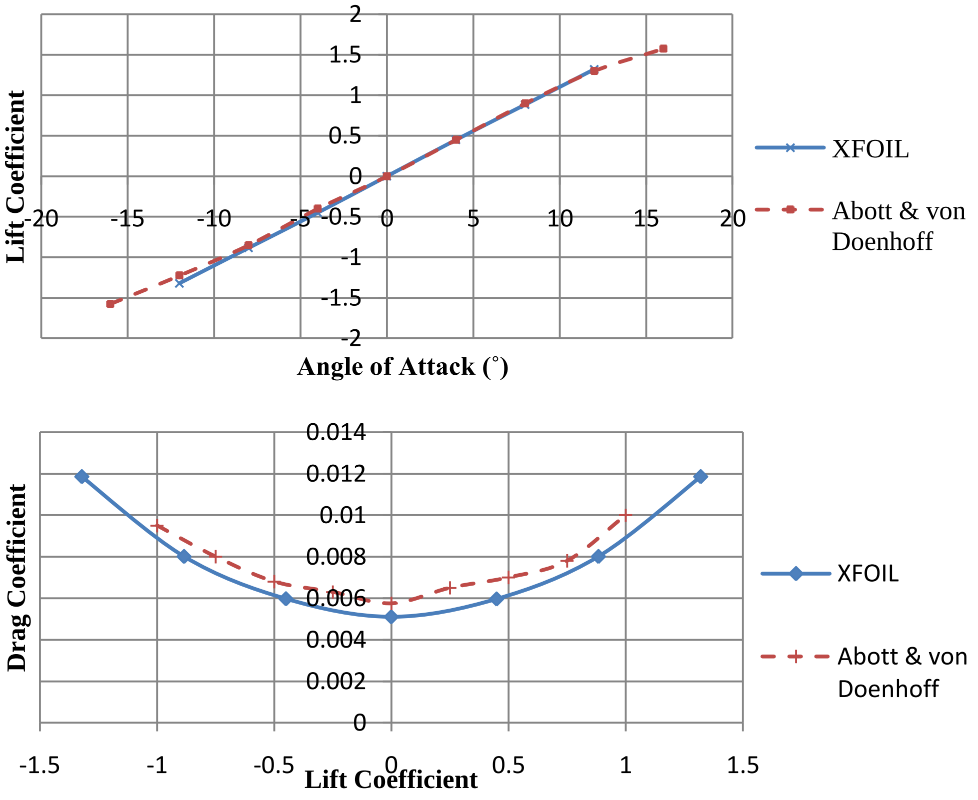

Figure 3: Comparison between XFOIL and Abbott and von Doenhoff[18]. C_L vs. Incidence (upper) and C_L vs. C_D (lower). Re = 6 Million.

4.2 Grid independence

In order to ensure that the 2D grids were independent of the number of grid points, several grids with an increasing number of cells were run and the drag coefficient was plotted for each case. The C_D was chosen as the case was a symmetrical airfoil at zero incidence, and additionally the drag is typically the quantity more difficult to obtain a correct value for than for other quantities, such as lift. In figure 3, it can be seen that for the case of an airfoil without trailing-edge extension using the S-A model, no significant

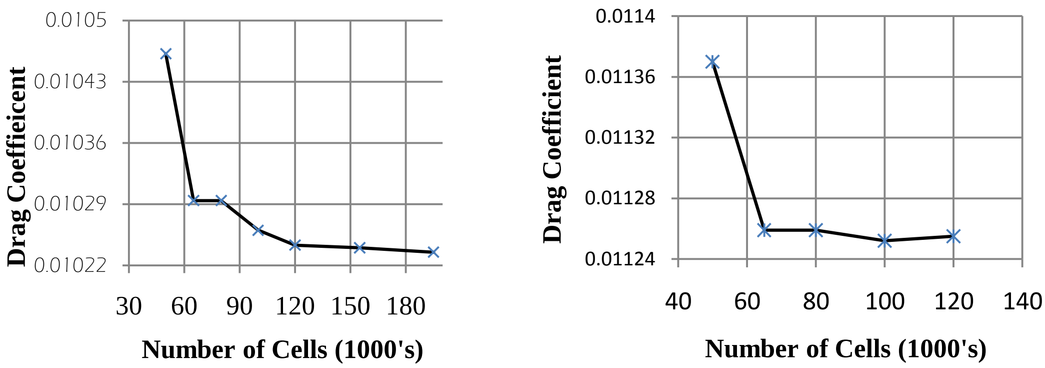

Figure 4: Grid independence study for 2D airfoil geometries using S-A model (left) and K-ε model for case including trailing-edge extension (right).

variation in the C_D value can be observed for meshes with more than 120,000 cells. When calculating the airfoil with splitter plate using the K-ε model, convergence was observed at 65,000 grid points. In addition, the value that the drag coefficient converges to within <1% error of the predictions obtained from XFOIL, giving confidence in the quality of the mesh and the numerical setup. The study was therefore taken forward to conducting three dimensional RANS of airfoils with serrated and unserrated trailing-edge extensions.

5 RESULTS

All cases conducted using the five turbulence models to be evaluated are tabulated in table 2. For a proper comparison between serrated and unserrated cases, a reference case, case D, was conducted with a trailing-edge extension length such that the overall area of the serrated and unserrated cases were equivalent.

Case	Dimensions	Case	Number of Cells
A.	2D	Clean airfoil	120,000
B.	2D	Airfoil with splitter plate with $l = 0.096$m	65,000
C.	3D	Clean airfoil	2,800,000
D.	3D	Airfoil with splitter plate with $l = 0.0465$m	5,500,000
E.	3D	Airfoil with splitter plate with $l = 0.096$m	7,000,000
F.	3D	Airfoil with serrated splitter plate	8,500,000

Table 1: Summary of cases; all airfoils are NACA-0012 geometry.

As already mentioned in the introduction, there exist no detailed data of the turbulent flow in the vicinity of trailing-edge extensions. Therefore, the solutions obtained with

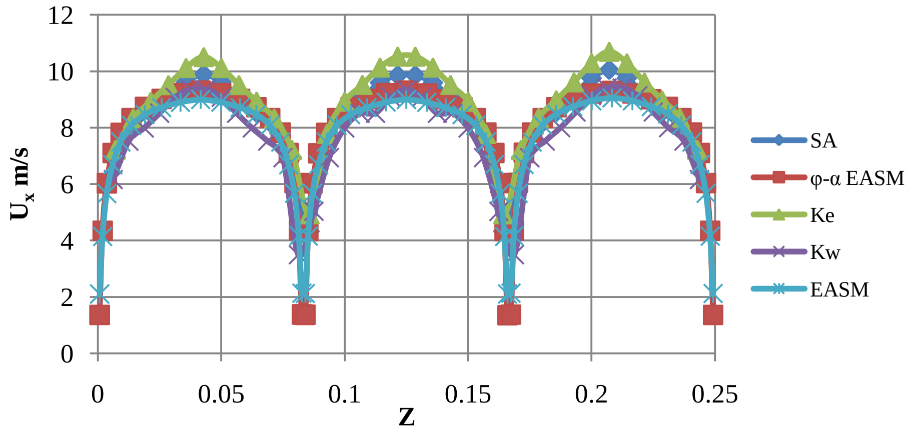

Figure 5: Spanwise distribution of the streamwise velocity component $\boldsymbol{U_x}$ for all tested turbulence models at the tip of the serrations.

various turbulence closures can only be compared to each other and to the unserrated reference case. In the following, the mean velocity and vorticity fields calculated with RANS will be compared. This is followed by an analysis of the turbulence viscosity predicted by all models.

5.1. Mean flow quantities

The first important observation to make was that the addition of trailing-edge serrations did virtually not increase the drag of the airfoils. The S-A model predicted C_D=0.010492 and C_D=0.010471 for cases D and F (see table 2), respectively; the K-ε model gave C_D=0.011531 and C_D=0.011550 for cases D and F, respectively; and the K-ω model gave C_D=0.010456 and C_D=0.010423 for cases D and F, respectively. Thus only in the case of using the K-ε model did the drag increase, but only by approximately 0.16%. When using the other two linear models, the drag was actually slightly decreased when adding trailing-edge serrations. For both EASM closures computed using OpenFOAM, the drag coefficient was not computed, but judging from the mean velocity fields there was no significant variation between serrated and unserrated cases.

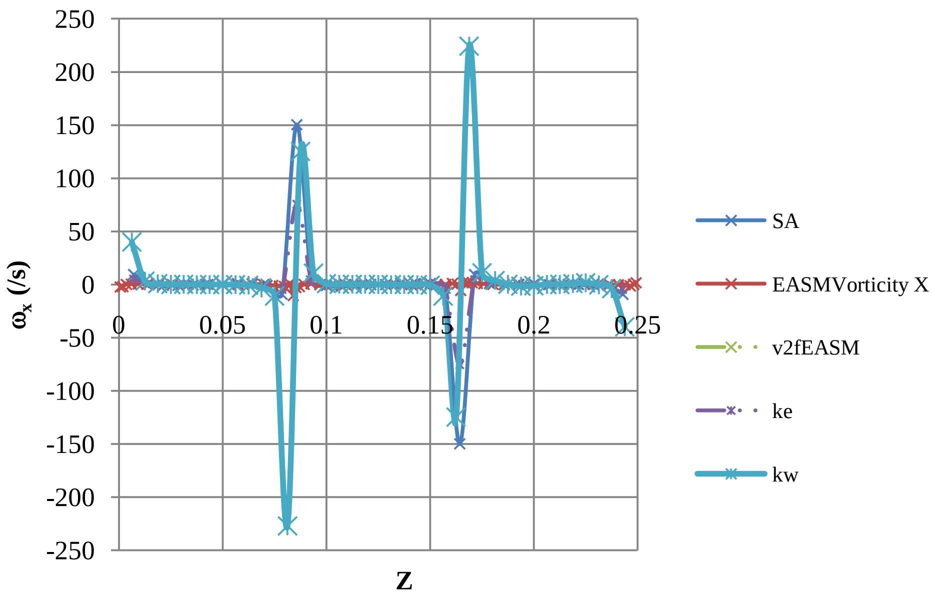

Figure 6: Spanwise distribution of the streamwise vorticity component ω_x for all tested turbulence models at the tip of the serrations.

The spanwise distribution of the streamwise velocity component, measured at the tip location of the serrations, is compared for all cases conducted in figure 5. A regular pattern governed by the regular spacing of the serration geometry can be observed for all cases, i.e. the flow velocity increases from its zero no-slip value on the serrations to a maximum between two tips. However, the maximum velocity varies between individual models, with the *K*-ε model and the EASM model predicting the highest and lowest velocities, respectively. It can also be noted, that the EASM-based models appear to predict a slightly flatter velocity distribution between the serration tips, i.e. there is not as pronounced a peak as for the other models used. Overall, the differences between the models are relatively small.

It is more instructive to look at the spanwise distribution of the streamwise vorticity component, ω_x, shown in figure 6. The first observation is that the vorticity levels are not the same for each serration but vary considerably from tip to tip. This is particularly visible for the case conducted using the *K*-ω SST model, which predicts the highest levels of vorticity. This asymmetric behaviour can be attributed to the presence of the spanwise boundary conditions, highlighting the importance of including more than one serration in the calculations. Both EASM variants predict much smaller values of vorticity than the linear eddy-viscosity based models. Without knowledge of what the

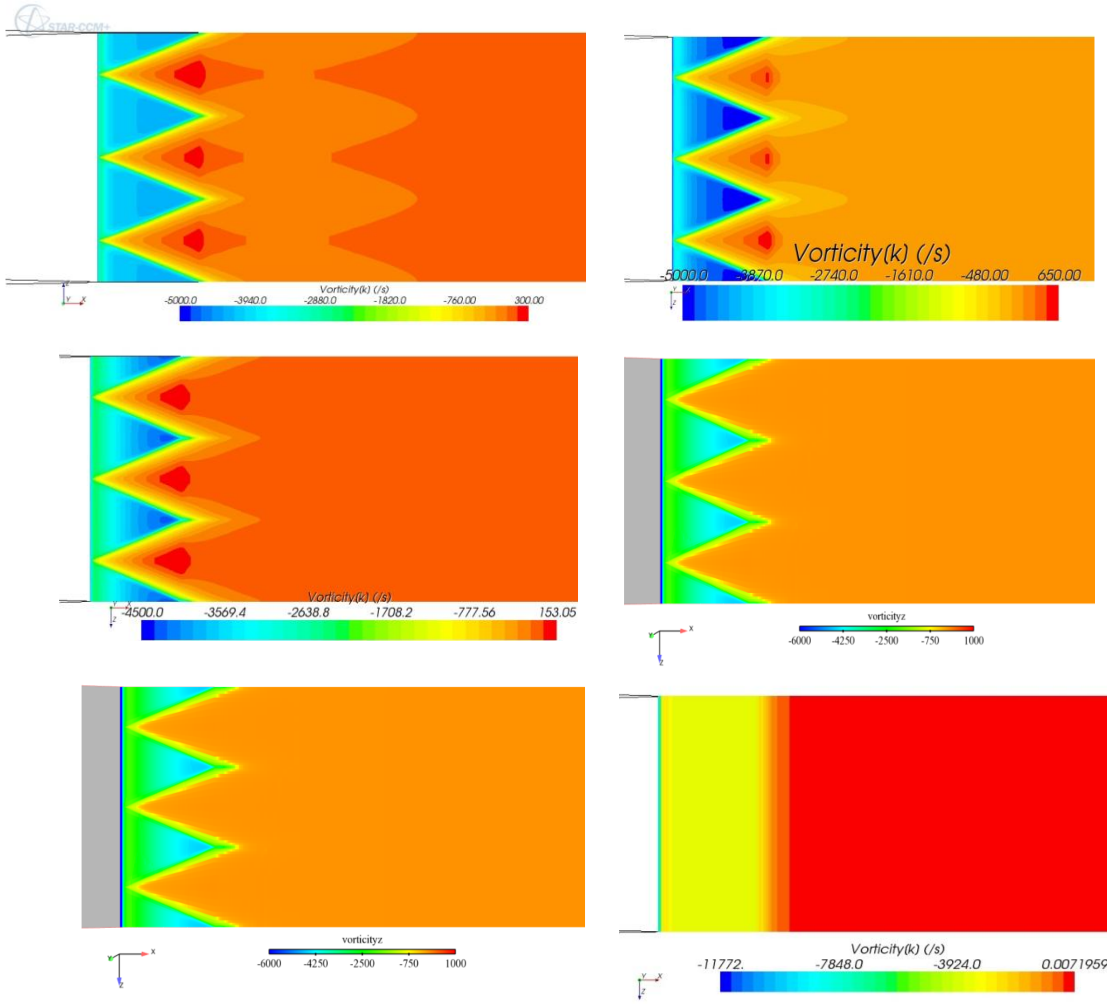

Figure 7: Contour plots of mean spanwise vortivity component ω_z. Top-view of the trailing-edge region, X-Z plane at Y=0.001m. Top left: S-A model; Top right: *K*-ε model; Middle left: *K*-ω SST; Middle right: EASM; Bottom left: φ-α EASM; Bottom right: S-A model for straight trailing edge. Note values are scaled to local maximum and minimum.

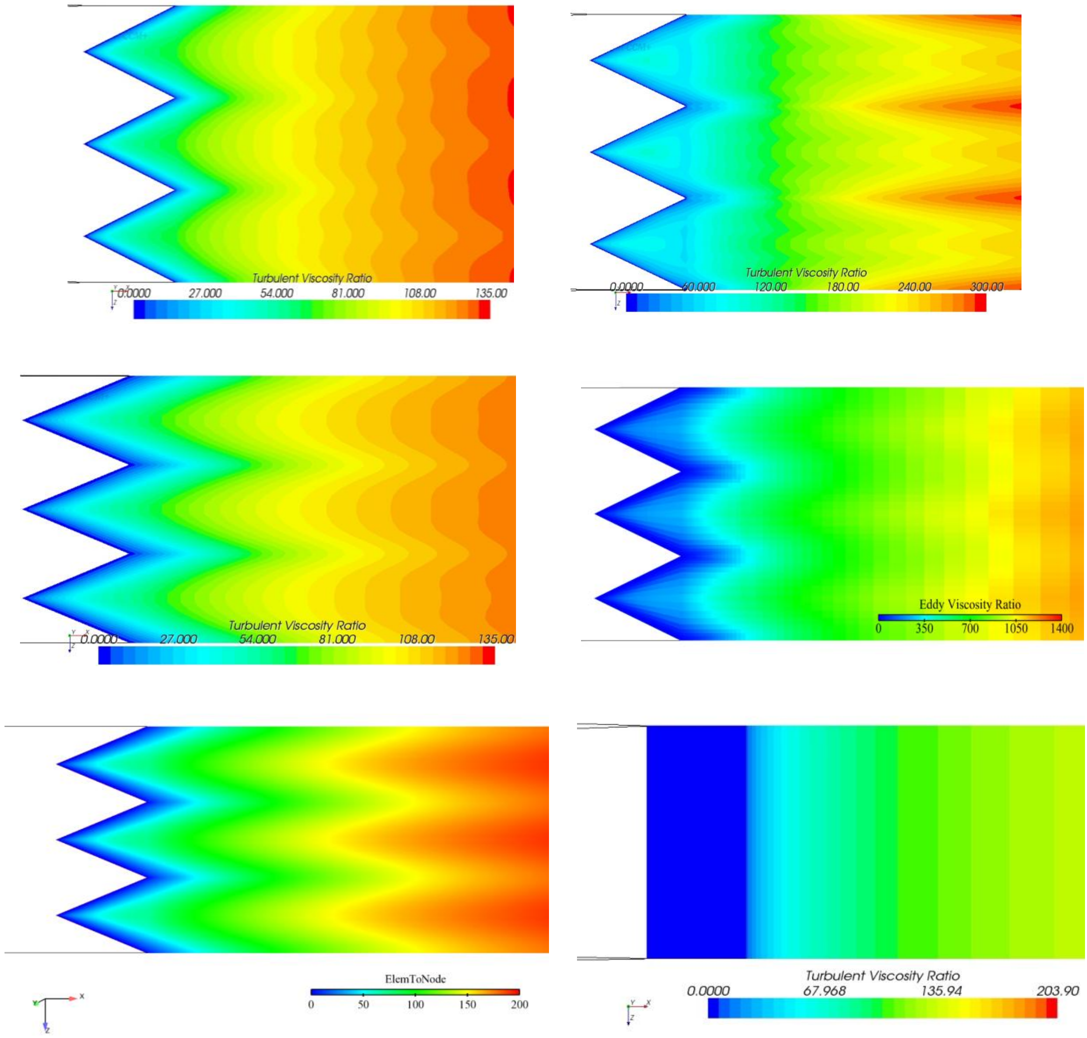

Figure 8: Contour plots of turbulence viscosity ratio. Top-view of the trailing-edge region, X-Z plane at Y=0.001m. Top left: S-A model; Top right: K-ε model; Middle left: K-ω SST; Middle right: EASM; Bottom left: φ-α EASM; Bottom right: S-A model for straight trailing edge. Note values are scaled to local maximum and minimum.

correct vorticity value should be, it can still be concluded from these results that any noise prediction method that requires the velocity gradient as input will be sensitive to the choice of turbulence model.

Finally, top-views of the spanwise vorticity component in an X-Z plane at Y=0.001m, corresponding to $Y^+\approx100$, above the trailing-edge extension are shown for all cases and an unserrated reference case in figure 7. The comparison highlights that all RANS models used predict strong variations between negative and positive spanwise vorticity component in the vicinity of the serrations; in contrast to the unserrated case, in which only a smooth transition from the negative values above the airfoil to small values in the wake can be observed. More importantly, the vorticity minima and maxima differ considerably from model to model, with the strongest variations observed for all linear models. In particular the K-ε model displays very strong variations between the areas above and between the serrations. Thus, judging already from mean flow variables and derived quantities, there are pronounced differences in the solutions dependent on the choice of the turbulence model.

5.1 Statistical quantities

All RANS-based noise prediction methods require turbulent length or velocity scales as input. Because for the current study the S-A model was to be included due to its popularity in the aerospace community, the only turbulence quantity that was available from all models used was the turbulence viscosity ratio. Top-views of the turbulence viscosity ratio in an X-Z plane at Y=0.001m, corresponding to $Y^{+}\approx100$, above the trailing-edge extension are shown in figure 8. In contrast to the mean flow results where the data obtained from difference RANS models differed only quantitatively, here qualitative differences between the results obtained from different RANS closures can be observed. Most turbulence closures employed predict small values of turbulence viscosity ratio close to the serrations with increased values between the teeth. This behaviour extends downstream and most models predict the peak values of the turbulence viscosity ratio downstream of the serration roots. However, for the K-ε model, the spanwise distribution of the turbulence viscosity ratio does not show significant spanwise variations close to the serrations and farther downstream the maxima are found downstream of the serration tips. The maximum value of turbulence viscosity ratio can be seen to vary strongly depending on the choice of turbulence model. The S-A model, K-ω SST and the φ-α EASM all predict similar levels, roughly the same values as those obtained in the unserrated case, while the K-ε model shows larger values downstream of the serrations and the EASM predicts very high levels throughout. In the DNS of Jones and Sandberg[12] it was observed that the maximum turbulence kinetic energy was between the serrations. This suggests that the behaviour predicted by the K-ε model is not correct. However, it should be noted that the Reynolds number and flow topology for the DNS conducted by Jones and Sandberg differ from the current case. In particular, the airfoil DNS conducted by Jones and Sandberg was turbulent on the upper surface only, whilst the lower surface boundary layer was laminar.

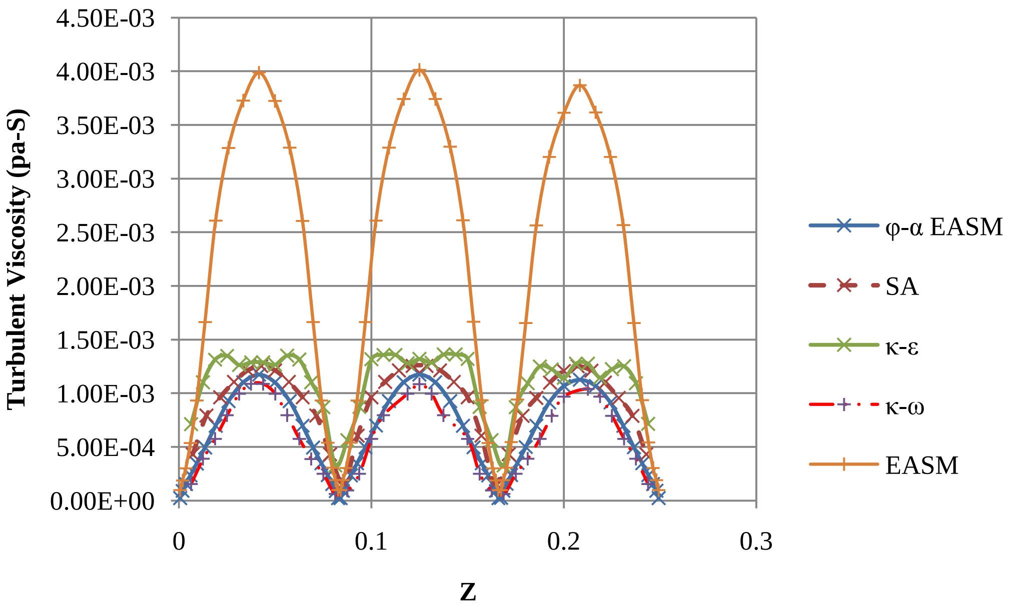

Figure 9: Spanwise distribution of the turbulence viscosity ratio for all tested turbulence models at the tip of the serrations.

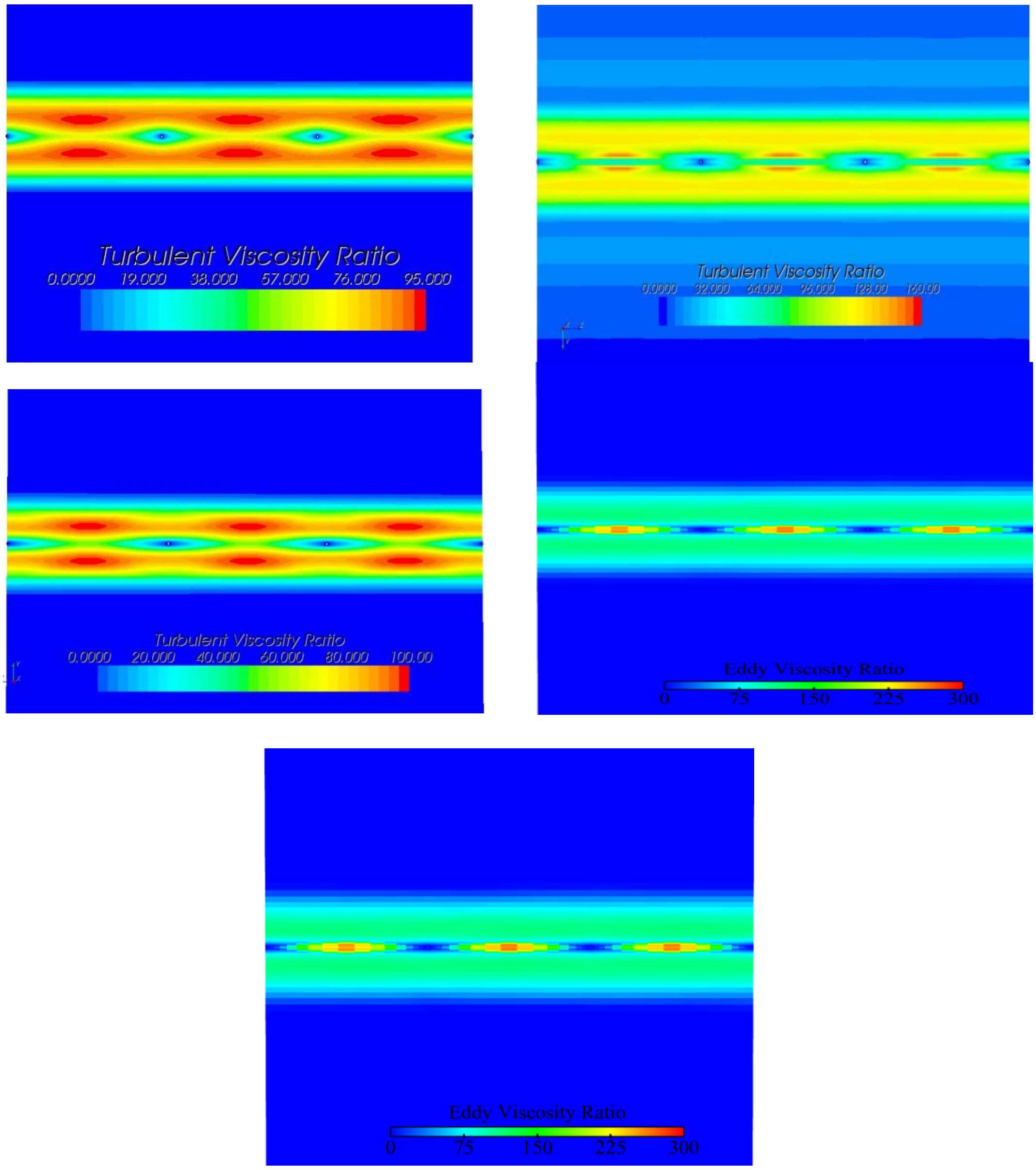

Figure 10: Contour plots of turbulent viscosity ratio. End-view of the trailing-edge region, Y-Z plane at X=1.096m. Top left: S-A model; Top right: K-ε model; Middle left: K-ω SST; Middle right: EASM; Bottom: φ-α EASM. Note values are scaled to local maximum and minimum.

For a more quantitative comparison, the spanwise distribution of the turbulence viscosity for all tested turbulence models is shown at the tip of the serrations in figure 9. It can clearly be seen that the K-ε model predicts a plateau-like distribution of the turbulence viscosity between the serrations while all other models predict a more pronounced peak. Also, the considerably higher values of the turbulence viscosity obtained using the EASM are highlighted. These large values obtained by the EASM might be due to a defect of the EASM model to predict a realistic value for C_μ in case of vanishing strain rates, a deficit that was addressed and appears to have been remedied in the φ-α EASM formulation. Overall, the S-A model, K-ω SST and the φ-α EASM all seem to predict similar distributions and values for the turbulence viscosity, implying that the strong deviations seen in the K-ε model and the EASM might be unphysical.

Finally, end-views of the turbulence viscosity ratio, shown in figure 10, were evaluated. The most striking difference observed is that for all linear models the highest values of the turbulence viscosity ratio is within the boundary layers, while both EASM variants appear to have a more localized distribution with maxima between the serrations at Y≈0. Originally, it was speculated that this behavior might be due to the use of the wall-distance in the dissipation terms of the K-ε and S-A models, as opposed to a fully wall-distance independent formulation of the EASM. However, the K-ω SST model exhibits the same behaviour as the two other linear models but is, in principle, wall-distance independent as well, except for the blending of the model coefficients.

Overall, the evaluation of the turbulence viscosity ratio shows that there are significant qualitative differences between the turbulence closures employed in this study. All models predict a strong spanwise variation of the turbulence viscosity and therefore might serve as an input for a RANS-based noise prediction tool. However, the fact that the statistical quantities predicted differ so strongly from model to model implies a considerable sensitivity of any noise prediction model to the choice of turbulence model.

6 CONCLUSIONS

Calculations of the flow over NACA-0012 airfoils at Re_C=1.06×10^6 with serrated and unserrated trailing-edge extensions have been conducted using five different RANS closures implemented in STAR CCM+ and OpenFOAM. The aim was to investigate the applicability of RANS-based turbulence models for accurate computation of the flow over trailing edge serrations in light of recently proposed RANS-based noise prediction models. Given the lack of detailed data of the flow in the vicinity of trailing-edge serrations from high-fidelity methods such as DNS, LES or laboratory experiments, the goal of this paper could not be to evaluate which turbulence closure gave the best results, but to evaluate whether there are significant variations in the solutions obtained from different models.

The first observation was that the addition of trailing-edge serrations did not increase the drag of the airfoils, a crucial requirement for any potential noise reduction technology. When looking at the mean streamwise velocity component, no significant differences between the RANS models could be observed. However, when scrutinizing the spanwise distribution of the streamwise vorticity component, ω_x, an asymmetric distribution with respect to the serration tips could be observed, implying that more than one serration should be included in the spanwise direction. Also, the vorticity maxima vary strongly from model to model, with the S-A and K-ω models predicting the largest values. In terms of the spanwise vorticity component , ω_z, the K-ε model displays very strong variations between the areas above and between the serrations.

The turbulence viscosity ratio was chosen for comparison in terms of statistical quantities because of the inclusion of the S-A model in this study. When comparing turbulence viscosity distributions obtained from various closures, qualitative differences could be observed. Most turbulence closures employed predict small values of turbulence viscosity ratio close to the serrations with increased values between the teeth and downstream of the serration roots. However, the K-ε model predicts maximum values downstream of the serrations tips which appears to contradict DNS results by Jones and Sandberg[12], although those results were at lower Reynolds numbers. However, the fact that the S-A model, K-ω SST and the φ-α EASM predict similar levels and distributions of turbulence viscosity increases trust in these models.

Lastly, end-views of turbulence viscosity ratio revealed that for all linear models the highest values of the turbulence viscosity ratio is within the boundary layers, while both

EASM variants appear to have a more localized distribution with maxima between the serrations at Y≈0.

Overall, it seems as if RANS closures are able to predict strong variations in the mean flow and statistical quantities due to the presence of trailing-edge serrations which is necessary to obtain a variation in a potential noise prediction. However, because the predicted values differ strongly depending on which turbulence model is employed, a considerable sensitivity of any noise prediction model to the choice of turbulence model is inevitable.

The first author would like to acknowledge financial support from the Aerodynamics and Flight Mechanics Research group of the School of Engineering Sciences and we thank Dr Lloyd Jones for his valuable comments.

REFERENCES

[1] T. Brooks, D. Pope, M. Marcolini, Airfoil Self-Noise and Prediction, NASA Reference Publication **1218** (1989)

[2] J. Ffowcs Williams, L. Hall, Aerodynamic sound generation by turbulent flow in the vicinity of a scattering half plane, *Journal of Fluid Mechanics* **40** (4) pp. 657-670 (1970)

[3] M.J. Lighthill, On sound generated aerodynamically I. General theory, *Proceedings of the Royal Society of London*, Series A Mathematical and Physical Science 211A (**1107**) 564-587 (1952)

[4] IUTAM Symposium on Computational Aero-Acoustics (CAA) for Aircraft Noise Prediction. http://iutam.org/ Last accessed March 2010.

[5]Oerlemans, S., Schepers, J.G. Prediction of Wind Turbine Noise and Validation Against Experiment. *International Journal of Aeroacoustics*, **8** (6), pp 555-584 (2009)

[6] F. Van den Berg, E Pedersen, J. Bouma, R. Bakker, WINDFARM perception: Visual and acoustic impact of wind turbine farms on residents – Final report (2008)

[7] Bohn, A. J., Edge Noise Attenuation by Porous-Edge Extensions, *AIAA Paper* 76-0080 (1976)

[8] Fink, M. R., and Bailey, D. A., Model Tests of Airframe Noise Reduction Concepts,”*AIAA Paper* 80-0979 (1980)

[9] Herr, M., Dobrzynski, Experimental investigations in low-noise trailing-edge design, *AIAA Journal* **43** (6) 1167-1175 (2005)

[10] M.S.Howe, Noise produced by a sawtooth trailing edge, *Journal of the Acoustical Society of America* **90**, pp 482 (1991)

[11] Oerlemans, S., Fisher, M., Maeder, T., and Kogler, K., Reduction of Wind Turbine Noise using Optimized Airfoils and Trailing Edge Serrations, *AIAA Paper*, 2008-2819 (2008)

[12] Jones, L & Sandberg R., Direct Numerical Simulations of Noise Generated by the Flow over an Airfoil with Trailing Edge Serration *AIAA Paper* 2009-3195 (2009)

[13] S. Glegg, B. Morin, O. Atassi, R. Reba., Using RANS Calculations of Turbulent Kinetic Energy to Provide Predictions of Trailing Edge Noise. *Paper* 2008-2993 (2008)

[14] R. Ewert, C. Appel, J. Dierke, M. Herr, RANS/CAA based prediction of NACA 0012 broadband trailing edge noise and experimental validation. *AIAA Paper* 2009-3269 (2009)

[15] Star CCM+ Version 4.04.011 User Manual

[16] Speziale, C. G., Sarkar, S., and Gatski, T. B., Modelling the pressure-strain correlation of turbulence: an invariant dynamical systems approach, *Journal of Fluid Mechanics*, **227**, pp. 245-272 (1991)

[17] Weinmann, M. and Sandberg, R. D., Suitability of Explicit Algebraic Stress Models for predicting complex three-dimensional flows, *AIAA paper* 2009-3663 (2009)

[18] Weinmann, M. and Sandberg, R. D., A new non-linear elliptic blending Reynolds-Averaged Navier-Stokes Model based on the inverse turbulent timescale. In preparation for *AIAA Journal*.

[19] M. Drela, XFOIL: An Analysis and Design System for Low Reynolds Number Airfoils, *Conference on Low Reynolds Number Airfoil Aerodynamics*, University of Notre Dame, (1989).

[20] Spalart, P.R. and Rumsey C., Effective Inflow Conditions for Turbulence Models in Aerodynamic Calculations, *AIAA Journal*, **45** (10), pp 2544-2553 (2007)

[21] Spalart, P.R. and Allmaras, S.R.,A One Equation Turbulence Model for Aerodynamic Flows, *Recherche Aerospatiale*, **1**, pp 5-21 (1994)

[22] Ira H. Abbott & Albert E. Von Doenhoff, Theory of Wing Sections, 1St Edition, *Dover* (1959)